Near-field infrared spectroscopy simulations using Altair Feko

P.McArdle, D.J.Lahneman, H.Jiang, M.M.Qazilbash – Department of Physics, College of William & Mary, Williamsburg, Virginia 23187-8795 / June 25, 2021

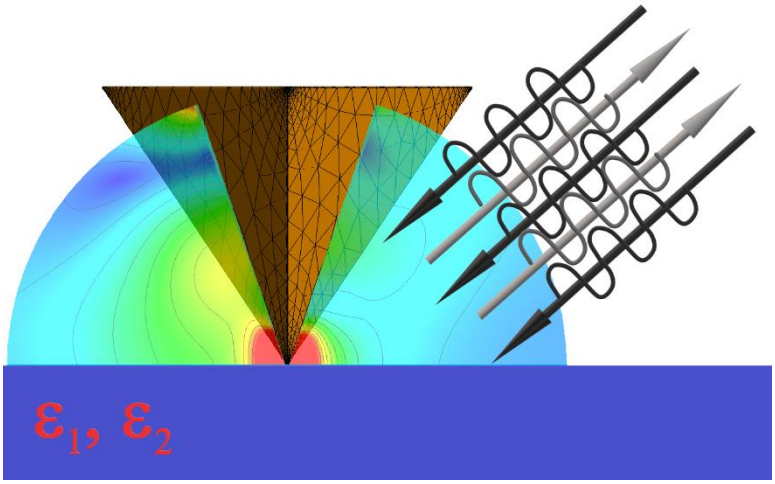

Introduction

In this white paper, we present our interesting research on novel numerical simulations of infrared nano-spectroscopy using Altair Feko which has been published in Physical Review Research [1]. We employed the Method of Moments (MoM) and Surface Equivalence Principle (SEP) solution methods to model experimental data. As a starting point, we will give a brief motivation for the experiment and physics, and why using simulations was necessary. The diffraction limit (figure 1.(b-d)) in optics, sets a bound on the spatial resolution obtainable in a spectroscopy or imaging experiment [2]. The diffraction limit is typically half of the incident wavelength being used in one's experiment. For mid and far-infrared wavelengths (~10 μm – 100 μm), this limits the spatial resolution and prevents the study of physics at nanometer length scale. Apertureless, scattering-type scanning near-field infrared microscopy (S-SNIM) [3] is an experimental technique that can circumvent the diffraction limit to study infrared properties at the nanoscale. It uses the tip of an atomic force microscope (AFM) to confine incident electromagnetic fields at the tip's apex (radius of curvature ~20 nm). The near fields from the tip are modified by the presence of a sample of interest. The modified fields from the tip, scatter light into the far field, which carry information about the sample's local optical properties. The spatial resolution that can be obtained is independent of the wavelength and is defined by the radius of curvature of the AFM tip apex (~20 nm). The outcome is up to 1000-fold increase in spatial sensitivity! We have used this technique to model and better understand surface phonon polaritons (SPhP) and their propagation. Surface polaritons result from the coupling of a high momentum photon and collective charge oscillations [4]. In S-SNIM, the tip is able to both excite and scatter SPhP information into the far-field. SPhPs are very interesting in part because of their potential applications in technologies such as optical addressing and data storage.

Challenges

To extract meaningful information from the experiment, we must model the complicated 3-dimensional scattering process of light from the tip-sample system. Simple analytical approximations exist that do not take into account the full geometry of the system. We chose to use Altair FEKO, to properly capture both the tip and sample geometries, which as we will show is extremely important to correctly reproduce experimental data. Initial computations were done on a personal computer. Due to the size and complexity of the calculations, computations were done primarily on the high performance computing center at the College of William & Mary. Depending on the complexity and size of a particular simulation, between 1 and 4 nodes of a sub-cluster containing between 8-16 cores/node were used.

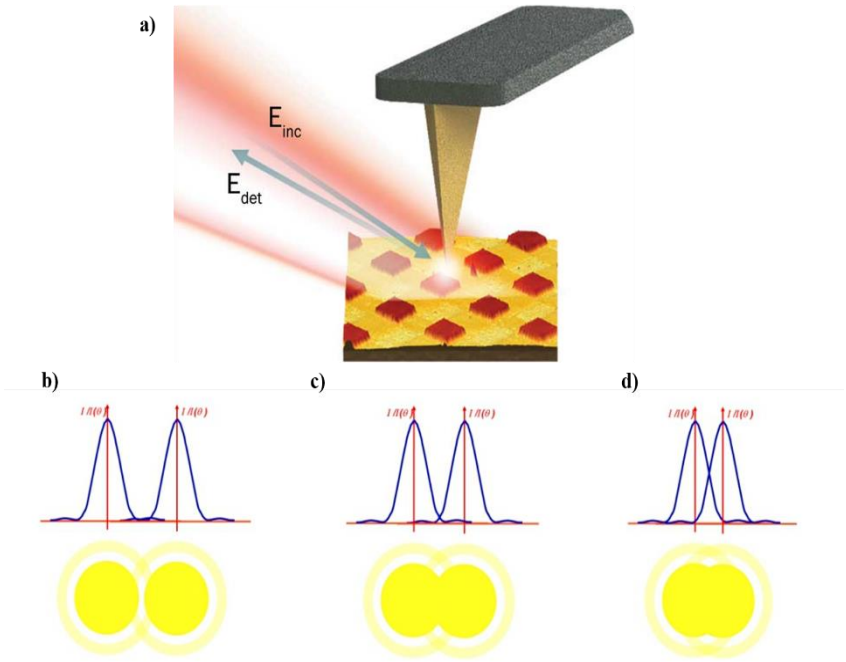

Figure 1 a) Interaction of light with tip-sample system in a scattering-type scanning near-field infrared microscope. The excitation source is focused on a tip (E_{inc}), the tip is brought into close contact with a sample. The sample modifies the near-fields of the tip, and backscatters this local information into the far-field (E_{dec}). b-d) Visual demonstration of the classical diffraction limit. b) Image from two distinguishable positions. These two points are clearly resolvable, as their Airy disks do not overlap. c) Two points are just resolvable-although the Airy disks overlap, they are separated by more than the Airy disk radius. d) These two points are not resolvable and lead to loss of spatial sensitivity. The figures are taken from ref [2].

Geometry Creation

Figure 2 shows the images of the AFM probe typically used in S-SNIM experiments. The AFM (Atomic force microscopy) probe consists of a tip, shaft, and cantilever. Since FEKO has an embedded Computer Aided Design (CAD) modeling interface and allows for the importing of externally generated models, we were able to generate an accurate model of our AFM probes[1]. To properly include the curvature at the tip apex, we obtained Scanning Electron Microscopy (SEM) images of the probe and extracted a 2-D outline of the apex from our SEM images. It extends approximately 150 nm up the tip length. A circular sweep of the outline was performed to generate a three-dimensional point cloud. This was fit to a Non-Uniform Rational B-Spline (NURBS) to form a closed surface. This was then connected smoothly to our tetrahedron with additional NURBS surfaces. Altogether, the geometric model is a detailed replica of the shaft and tip of our probe. The cantilever has been omitted from the geometric model because it has negligible influence on the simulated tip-sample near-field interaction. The commercially available AFM tips generally used in experiments are composed of silicon coated with a thin metallic layer.

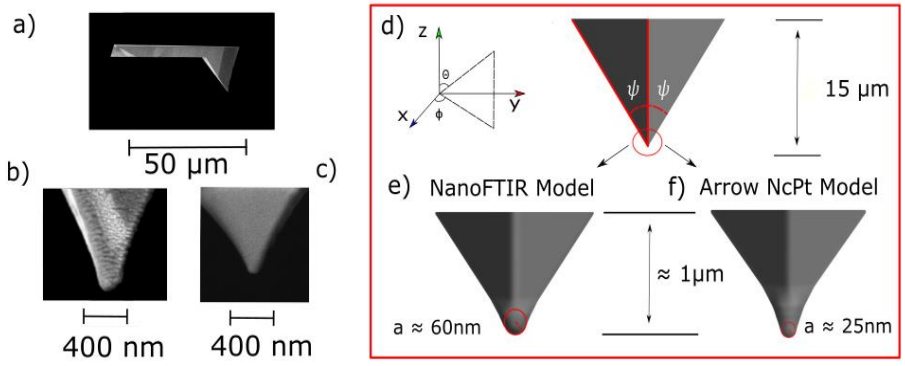

Figure 2- a) SEM image of the entire AFM nano-FTIR probe consisting of tip, shaft, and cantilever. b) Higher resolution SEM image of the nanoFTIR tip apex. c) High resolution SEM image of Arrow tip whose apex has a smaller radius of curvature compared to nanoFTIR d) Tetrahedral shaft with full angle $\psi \sim 60^{\circ}$ based on the SEM images which is used in both probe models. The tip apex within the red circle is shown in panels (e) and (f). (e) Geometry of the nanoFTIR tip apex with radius of curvature a ~ 60 nm. f) Geometry of the Arrow tip apex with radius of curvature a ~25 nm tip.

Problem Formulation

To reduce computational complexity in our numerical simulations, we assume the tip is a perfect electrical conductor (PEC). The simulation methods used were the method of moments (MoM) and surface equivalence principle (SEP) coupled with a half-planar/multilayered Green's function. The MoM is well suited for solving radiation and scattering problems. We only meshed the scatterer's surface, which greatly reduces the computation time. Application of the MoM allows the use of a planar or multilayered Green's function which is an accurate and efficient approach to computing near-field contrast of bulk isotropic materials. In our simulations, we employed the probe geometries in figure 2, above an isotropic half-planar sample. Isotropic materials have optical properties that are independent of the incident excitation fields. A plane wave is incident at φ= 45˚, θ= 60˚ and extends throughout the solution space which is a 1 mm x 1 mm x 1 mm cube. We demonstrate that these simulations provide a good quantitative description of the experimental spectra when the experimental spectra are normalized to a reference material like gold (Au) or silicon (Si), or when the experimental spectra are obtained without normalizing to a reference material[1]. The details about the experiments are given in Refs. 1 and 5.

An incident plane wave illuminates the tip-sample system and the scattered far-field is computed in the same direction as the incident plane wave. The scattered fields are simulated across a specified spectral bandwidth and with the tip at different discrete positions above the sample. These positions are determined by taking into account the tapping amplitude and frequency used in the experiments. In the experiment, the AFM tip is operating in tapping mode. The near field in the tip-sample gap is nonlinear in the tip-sample distance. Working in tapping mode, the scattered fields can be decomposed into a Fourier series. The higher order terms in the Fourier series represent pure near-field contributions independent of background scattering processes. Having simulated the scattered fields as a function of tip position and frequency, the following parametrization is used to mirror the fields in time in order to make them periodic.

$$z(t) = \frac{A}{2}(1 + cos(\Omega t)) \quad (1)$$

Here $\Omega = 2\pi\tilde{\nu}$ and $\tilde{\nu}$ is the tip oscillation frequency. The incident and scattered electric fields have frequency dependence ν and the scattered electric field is periodic in time due to the oscillating tip. Hence, one can expand the scattered electric field into a Fourier series

$$E_{scat}(t, \nu) = \sum_{n=0}^{\infty} c_n(\nu) * e^{i*2\pi n\tilde{\nu}t} \quad (2)$$

Employing the Fourier transform method, one can solve for the complex valued coefficients

$$c_n(\nu) = \frac{1}{T}\int_0^T E_{scat}(t,\nu)e^{-i2\pi n\tilde{\nu}t}dt \quad (3)$$

Where T= 2π/Ω is the period of tip oscillation. From these coefficients one obtains the field amplitude s_n and phase ϕ_n that are sampled in the far-field

$$c_n = s_n e^{i\phi_n} \ , s_n = |c_n| \ , \ \phi_n = tan^{-1}\left|\frac{Im(c_n)}{Re(c_n)}\right| \quad (4)$$

For referenced near-field amplitude and phase contrast, the simulation is performed on both a sample of interest and a reference material. This results in the following near-field contrasts

$$\frac{c_n^{sample}}{c_n^{ref}} = \frac{s_n^{sample}}{s_n^{ref}} \, e^{i(\phi_n^{sample} - \phi_n^{ref})} \quad (5)$$

Where the ratio $\frac{s_n^{sample}}{s_n^{ref}}$ is the demodulated near-field amplitude contrast and $(\phi_n^{sample} - \phi_n^{ref})$ is the demodulated near-field phase contrast.

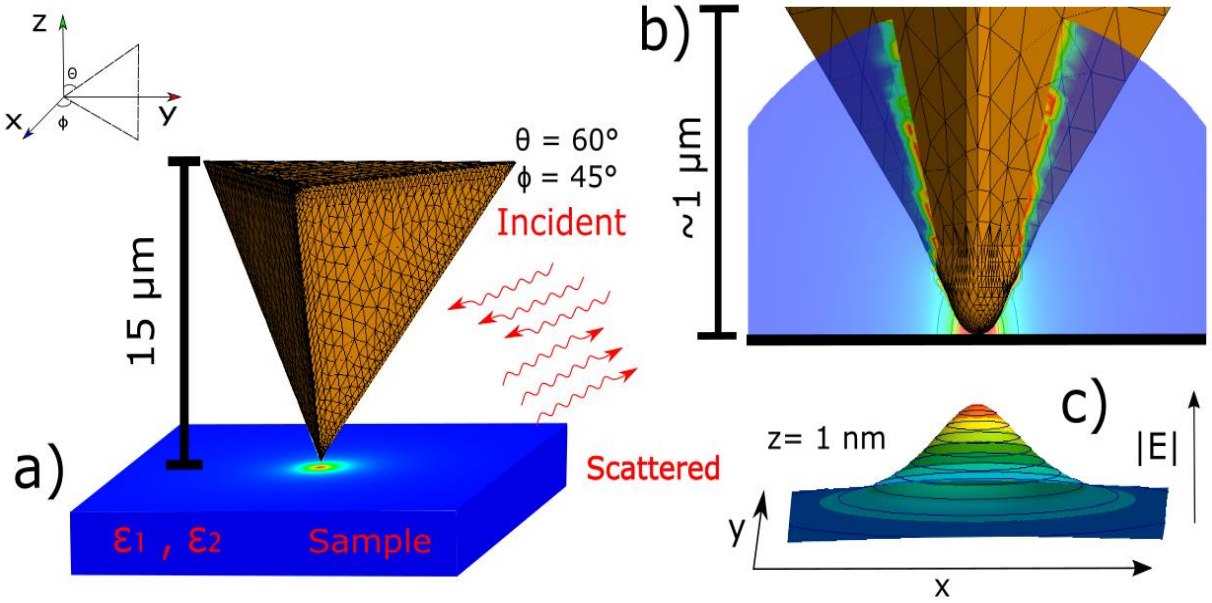

Figure 2 – a) A schematic representation of the simulation showing the meshed AFM nanoFTIR probe, the sample, and the incident and scattered electromagnetic fields. The sample's dielectric function has real and imaginary parts ε_1, ε_2 respectively. A fine mesh was used near the tip apex and a coarse one far from it. b) Front side schematic of the AFM probe near the tip apex over an infinite Au sample and computed electric field distribution. The probe shown in panels a-b is meshed as it was in simulations presented in this work. c) Plot of the computed electric field distribution as a function of x-y spatial position at a fixed z position of 1 nm over an infinite Au sample with the probe at a height of 10 nm above the sample. The electric field is computed at a frequency of 438 cm^{-1}.

Results

For a demonstration of the simulations, we present figures 4 & 5. The experimental data and Feko simulations displayed in figure 4 are obtained on 100 nm of SiO_2 on Si normalized to Si. The more interesting case is displayed in Figure 5 where two separate SPhPs are present. The resonance features are SPhP resonances, which we are able to capture accurately in both amplitude and phase, using the simulation techniques outlined in the text.

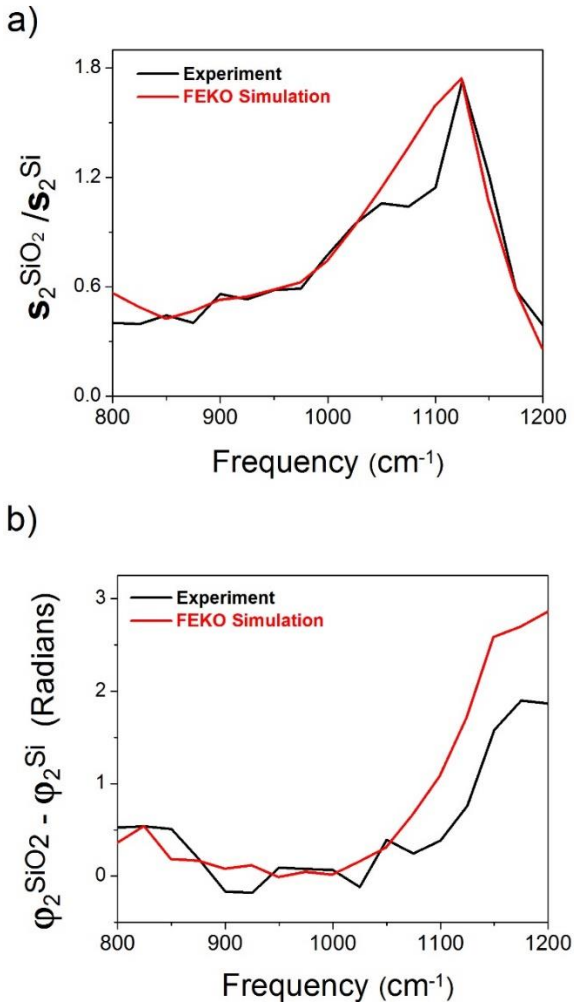

Figure 4 – a) The n=2 near-field amplitude spectrum and b) phase spectrum of 100 nm thick SiO_2 on Si normalized to the spectra of Si. The experimental data is shown along with results from numerical FEKO simulations.

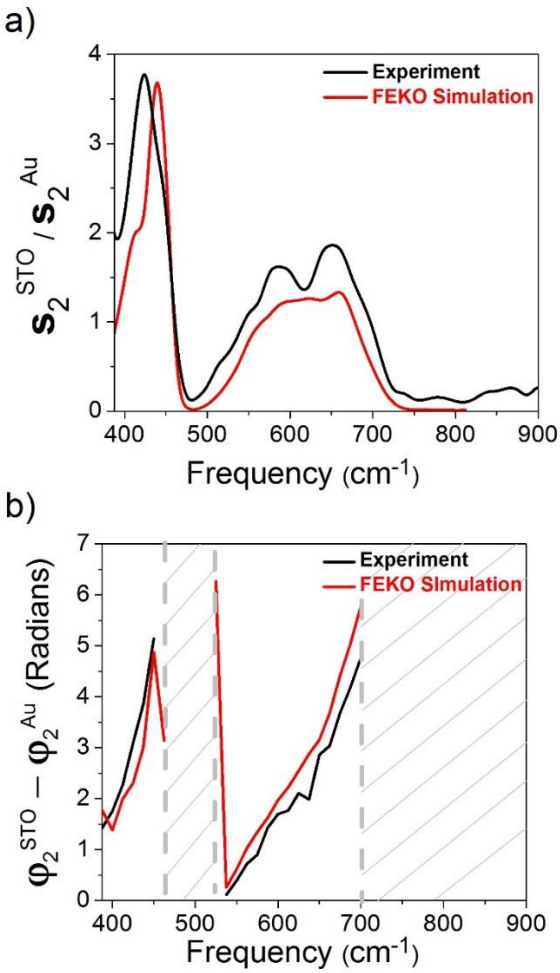

Figure 5 – a) The n=2 near-field amplitude spectrum and b) phase spectrum of bulk $SrTiO_3$ (STO) normalized to the spectra of Au. The experimental data is shown along with results from numerical FEKO simulations. The phase is indeterminate in the spectral regions depicted by the gray hatched areas in b), because the scattering amplitude from STO is negligibly small in these spectral regions.

Conclusion

In conclusion, we have developed a numerical technique to accurately model the experimental near-field amplitude and phase spectra in near-field infrared nano-spectroscopy. Our numerical method is especially useful for describing surface phonon-polaritons. Also, extension of our numerical technique to materials with anisotropic dielectric function and/or heterogeneous structure is possible in the future. This method is efficient to elucidate fundamental physical phenomena measured in near-field infrared nano-spectroscopy experiments on novel, complex materials.

References

[1] McArdle, P., Lahneman, D. J., Biswas, A., Keilmann, F., & Qazilbash, M. M. Physical Review Research, 2(2), 023272 (2020).

[2] Lipson, A., Lipson, S. G., & Lipson, H. (2010). Optical physics. Cambridge University Press.

[3] Keilmann, F., & Hillenbrand, R. Philosophical Transactions of the Royal Society of London. Series A: Mathematical, Physical and Engineering Sciences, 362(1817), 787-805 (2004).

[4] Huber, A., Ocelic, N., Kazantsev, D., & Hillenbrand, R. Applied physics letters, 87(8), 081103 (2005).

[5] Lahneman, D. J., Huffman, T. J., Xu, P., Wang, S. L., Grogan, T., & Qazilbash, M. M. Optics Express, 25(17), 20421-20430 (2017). .